

## RESEARCH ARTICLE

# A Compact Gap-Waveguide Dual-Polarized Ka-Band Feed for 50dBi Reflector Antennas With Tracking Function

ENLIN WANG<sup>1,2</sup>, TIANLING ZHANG<sup>1,2</sup>, (Member, IEEE),  
ASHRAF UZ ZAMAN<sup>1</sup>, (Senior Member, IEEE), THOMAS EMANUELSSON<sup>3</sup>, (Member, IEEE),  
PER-ARNE THORSEN<sup>4</sup>, SAM AGNEESSENS<sup>5</sup>, AND JIAN YANG<sup>1</sup>, (Senior Member, IEEE)

<sup>1</sup>Department of Electronic Engineering, Chalmers University of Technology, 41296 Gothenburg, Sweden

<sup>2</sup>Department of Electronic Engineering, Xidian University, Xi'an 710071, China

<sup>3</sup>Department of Transport Systems, Ericsson AB, 41756 Gothenburg, Sweden

<sup>4</sup>Department of Transport Products, Ericsson AB, 41756 Gothenburg, Sweden

<sup>5</sup>Department of Research, Ericsson AB, 41756 Gothenburg, Sweden

Corresponding author: Jian Yang (jian.yang@chalmers.se)


This work was supported by the Strategic Innovation Program "Smarter Electronics Systems," a Joint Venture of Vinnova, Formas and Energy Agency, under Grant 2021-01354.

**ABSTRACT** A dual-polarized Ka-band feed based on gap waveguide (GW) technology for an ultra-high-gain reflector antenna is presented. The feed provides SUM-beams for data transfer and DIFF-beams for tracking. The whole reflector antenna is composed of the feed and a dual-reflector Cassegraine antenna. The feed has been prototyped, and the measured reflection coefficients for the horizontally and the vertically polarized SUM-beam ports are below  $-10$  dB and  $-8$  dB over 30.8 – 38 GHz, respectively. The measured feed radiation patterns agree well with the simulated ones. The dual-reflector Cassegraine antenna has been designed and simulated by using GRASP with the simulated far-field function of the proposed feed, showing that the reflector antenna achieves SUM-beam gains above 50 dBi and the null depth of the DIFF-beams are more than 30 dB below the maximum of SUM-beams.

**INDEX TERMS** Dual-polarized feed, gapwave planar magic-T, feed with tracking functions, ultra-high-gain antenna.

## I. INTRODUCTION

5G and beyond 5G wireless communication systems will provide ultra-fast data transfer up to 10 Gbps with an ultra-low latency of 1 ms, which can be realized only inevitably with the support of millimeter wave (mmWave) systems. Delivering high data rate in mmWave backhauling (point-to-point) systems over long distances is a big challenge due to the severe path loss and other limitations. Since it is not economically viable to deploy backhaul systems with station towers within every hundred meters, ultra-high gain ( $\geq 50$  dBi) antennas operating at mmWave regime are the core to implement

The associate editor coordinating the review of this manuscript and approving it for publication was Kai-Da Xu .

5G mmWave backhauling systems sustainably with a long-distance coverage [1].

However, the ultra-high antenna gain means ultra-narrow beamwidth (50dBi gain requires a narrow 3-dB beamwidth of about  $0.6^\circ$ ), where vibrations and wind loads on the antenna may cause the antenna beam swing and result in disruption of the link. Therefore, the beam tracking becomes a critical requirement for mmWave backhauling ultra-high-gain antennas.

Among tracking techniques, the monopulse tracking with comparators to provide SUM and DIFF patterns is widely used due to its accurate performance [2]. Most of monopulse comparators are made of 3-dB couplers, phase shifters or magic-Ts [3], [4], [5], [6], [7], [8], [9], [10], [11], [12], [13]. In [3], a comparator was realized by using groove gap

waveguide (GGW) magic-Ts with a complicated two layers. In [5], substrate-integrated-waveguide (SIW) based magic-Ts were employed to form comparators, which increases dielectric loss in mmWave regime. Hollow-waveguide based magic-Ts exhibit good performance, such as low loss and wide bandwidth [6], but with complex 3-D geometries and therefore high cost at mmWaves [14]. Several planar structured magic-Ts were proposed [15], [16], [17]. Using the low-temperature co-fired ceramic (LTCC) technology, planar magic-Ts can be designed through microstrip-line-slot transition and aperture coupling structure [16], but still with high loss at mmWaves.

The purpose of our work is to design a dual-polarized feed for a dual-reflector Cassegraine antenna of an ultra-high gain above 50 dBi with a compact geometry and a low manufacture cost at Ka-band. The GW technology is characterized by low losses, contactless layered structures and therefore low manufacture costs and easy assembling. Many mmWave GW antennas and passive components have been reported [18], [19], [20], [21], [22], [23]. As for monopulse antennas, radial line slot arrays (RLSAs) combined with a GW feeding network achieved monopulse characteristics but with only a very narrow band [22]. In [23] and [24], a monopulse network using Butler matrix was implemented based on the GW technology. However, all reported GW monopulse antennas including aforementioned are either single linearly or single circularly polarized. In [25] and [26], dual-polarized array antennas based on GW technology at Ka-band and W-band were presented respectively without monopulse function.

In this paper, a new dual-polarized broadband monopulse GW feed for a dual-reflector Cassegraine antenna at Ka-band is proposed. The dual-reflector Cassegraine antenna was preliminarily designed in order to verify that the feed can operate well in the antenna system with good radiation patterns. The performance of the whole antenna is simulated with a commercial solver, GRASP [27], using the CST [28] simulated far-field functions of the feed, verified by measurements, to show preliminary results of the ultra-high-gain antenna for 5G backhauling systems. The novelties of this work include: 1) A square radiation horn with new feeding structure of dual polarization with good isolation between polarizations, low cross polar level and good impedance matching realized by GW technology; 2) A new compact planar magic tee with three ridged gap waveguide (RGW) branches and one E-plane groove gap (E-GGW) branch has been proposed, and the magic tee with three E-GGW branches and one RGW branch proposed in [29] and [30] has been simplified for easy manufacture; 3) Two single-layered comparators, each for one polarization, realized by three contactless metal plates with several new GW transitions between layers for low cost manufacturing and easy assembling; 4) A dual-polarized simple layered structured monopulse feed.

This paper is organized as follows. Section II presents the feed design with simulation and measurement data. Section III describes the preliminary design of the dual-reflector Cassegraine antenna with the designed feed and

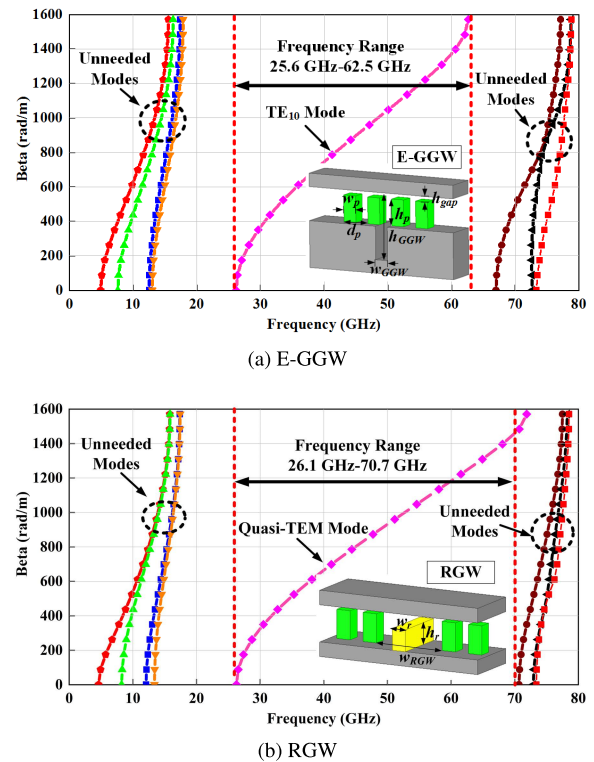


**FIGURE 1. Geometries and dispersion diagrams of two gap waveguides: E-GGW and RGW with dimensions as  $h_{\text{gap}} = 0.05$  mm,  $h_p = 2.0$  mm,  $w_p = 1.0$  mm,  $d_p = 2.0$  mm,  $h_{\text{GGW}} = 4.5$  mm,  $w_{\text{GGW}} = 1.0$  mm,  $h_r = 1.75$  mm,  $w_r = 0.8$  mm,  $w_{\text{RGW}} = 2.0$  mm.**

presents simulated performance. Section IV draws conclusions of the work.

## II. DESIGN, FABRICATION AND MEASUREMENTS OF THE MONOPULSE FEED

In order to describe the geometry of the feed more clearly, we define that a plate is a metal one with texture patterns on one side or both sides and a layer is the space between two plates. The waves propagate in layers (or in other words, between plates). The feed is of a geometry with two layers made by three plates.

### A. TWO TYPES OF GAP WAVEGUIDES

For a compact geometry, the combination of two types of GWs is used in the comparator: the E-GGW and the RGW. The geometries of the E-GGW and the RGW are given in Fig. 1, with dimensions in the caption. The dispersion diagrams are calculated by using the Eigen-mode solver of CST Microwave Studio. It is seen that the E-GGW and the RGW achieve a single Quasi-TEM mode transmission over 25.6 – 62.5 GHz and 26.1 – 70.7 GHz, respectively.

### B. MONOPULSE COMPARATOR

Two types of wideband planar magic-Ts based on the GW technology, the 3(RGW)+(E-GGW) Magic-T and the

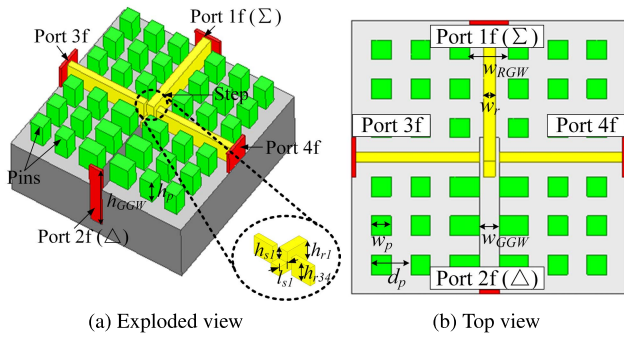
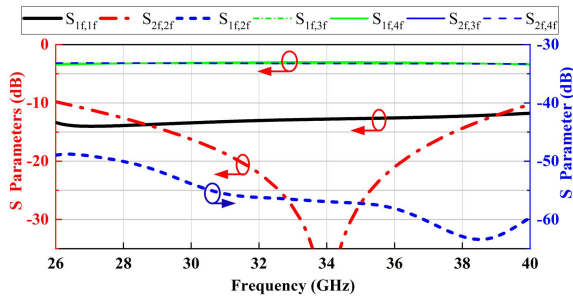
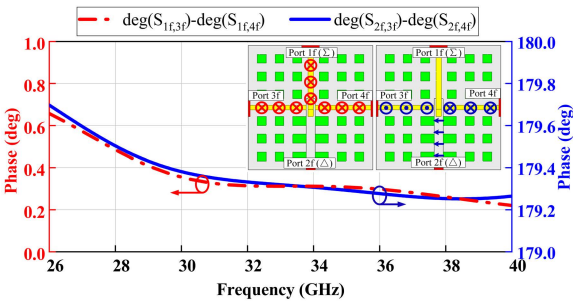


**FIGURE 2.** 3(RGW)+(E-GGW) Magic T, where the upper plate is hidden for clarifying, with dimensions as  $h_{r1} = 1.75$  mm,  $w_{RGW} = 2$  mm,  $h_{r34} = 1.5$  mm,  $h_{s1} = 0.6$  mm,  $l_{s1} = 0.4$  mm,  $w_r = 0.5$  mm.



(a) Magnitude of S-parameters



(b) Phase of S-parameters

**FIGURE 3.** Simulated results of 3(RGW)+(E-GGW) Magic T.

3(E-GGW)+(RGW) Magic-T, are proposed in order to form a compact monopulse comparator.

Fig. 2 shows the geometry of the 3(RGW)+(E-GGW) planar magic-T that is composed of three RGWs and an E-plane GGW. The work principle is illustrated in Fig. 3. When Port 1f is excited, the signal from Port 1f will be split with the equal magnitude and in-phase into Port 3f and Port 4f, where a capacitive coupling is applied. When Port 2f is excited, the signal from Port 2f will be split with the equal magnitude and out-of-phase into Port 3f and Port 4f via the capacitive gap and help of a cavity below the extended ridge. By adjusting the parameters  $l_{s1}$  and  $h_{s1}$  of the junction, a good impedance matching performance can be obtained. Fig. 3 shows the simulated results of the 3(RGW)+(E-GGW) magic-T. Within the frequency band of 26–40 GHz, the reflection coefficients at Port 1f and Port 2f are below  $-10$  dB, the isolation between

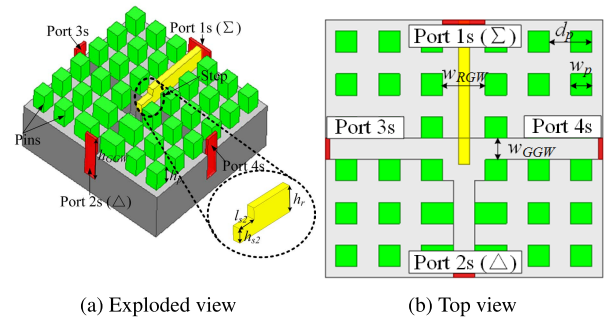
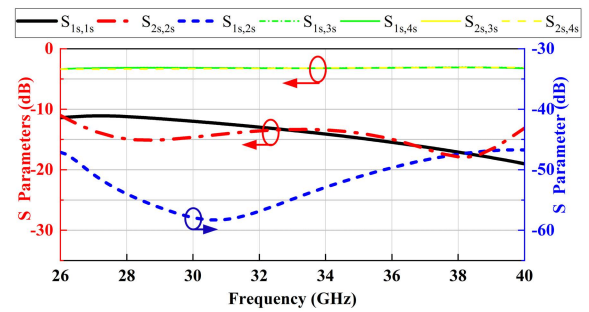
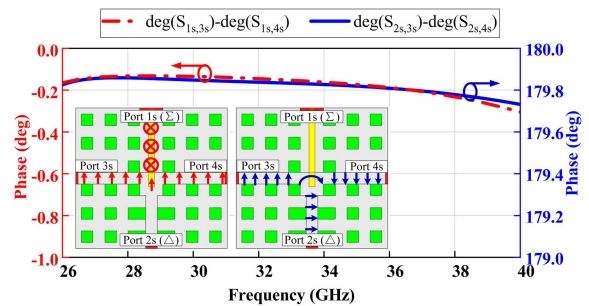


**FIGURE 4.** 3(E-GGW)+(RGW) Magic T, where the upper plate is hidden for clarifying, with dimensions as  $h_{s2} = 0.5$  mm,  $l_{s2} = 0.7$  mm,  $w_m = 2.0$  mm,  $l_m = 1.0$  mm.



(a) Magnitude of S-parameters



(b) Phase of S-parameters

**FIGURE 5.** Simulated results of 3(E-GGW)+(RGW) Magic T.

the two ports is better than 45 dB, and the phase imbalance due to numerical errors in CST is found less than  $0.8^\circ$ .

Fig. 4 illustrates the geometry of the 3(E-GGW)+(RGW) planar magic-T, correspondingly consisted of three E-GGWs and an RGW. The work principle illustrated in Fig. 5 is similar to that of the 3(RGW)+(E-GGW) magic-T. A similar performance, i.e., below  $-10$ dB reflection coefficients at Ports 1s and 2s, better than  $-45$ dB isolation between the two ports,  $0.3^\circ$  phase imbalance error is also obtained over 26–40 GHz, as shown in Fig. 5.

The monopulse comparator is realized by combining one 3(RGW)+(E-GGW) magic-T, two 3(E-GGW)+(RGW) magic-Ts and an E-plane T-junction divider, as shown in Fig. 6, with three ports: SUM Port $_{\Sigma}$ , E-plane DIFF Port $_{\Delta E}$ , and H-plane DIFF Port $_{\Delta H}$ . Fig. 7 shows the electric

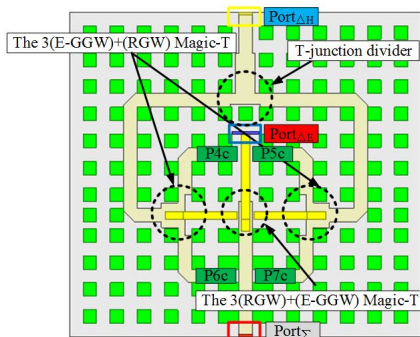
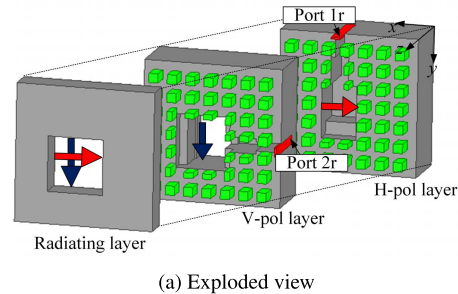
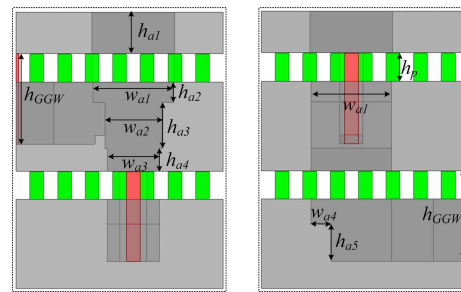


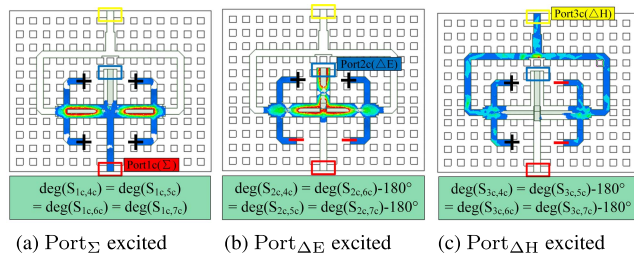
FIGURE 6. Proposed monopulse comparator, where P4c - P7c are ports to feed radiation elements.



(a) Exploded view



(b) Side views from Port 1r (left) and from 2r (right)



(a) Port $_{\Sigma}$  excited (b) Port $_{\Delta E}$  excited (c) Port $_{\Delta H}$  excited

FIGURE 7. Electric field distribution of the proposed monopulse comparator at 34 GHz.

FIGURE 9. Geometry of the radiation element, with dimensions as  $h_{a1} = 3$  mm,  $h_{a2} = 1.5$  mm,  $h_{a3} = 4$  mm,  $h_{a4} = 1.6$  mm,  $h_{a5} = 2.7$  mm,  $w_{a1} = 6$  mm,  $w_{a2} = 4$  mm,  $w_{a3} = 3.8$  mm,  $w_{a4} = 1.5$  mm.

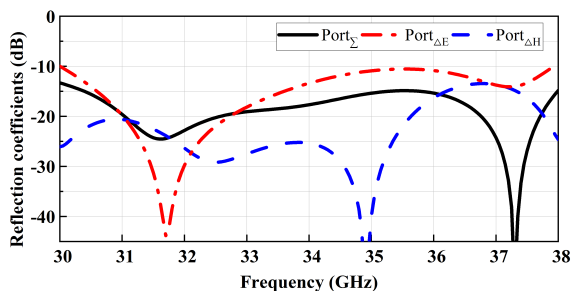


FIGURE 8. Simulated S parameters of the proposed comparator.

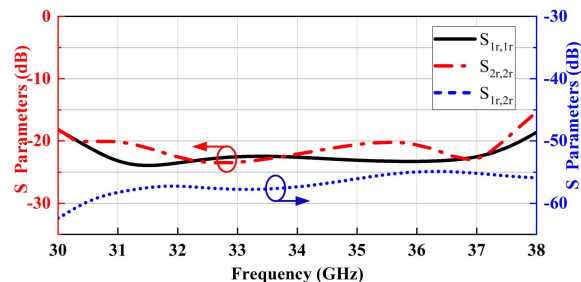


FIGURE 10. Simulated reflection coefficients and mutual coupling between dual-pol ports of radiation element.

field distribution of the proposed monopulse comparator at 34 GHz. The signal from SUM Port $_{\Sigma}$  propagates through the 3(RGW)+(E-GGW) magic-T first, and then the 3(E-GGW)+(RGW) magic-T to Ports 4c-7c with equal magnitude and same phase, while the signal from Port $_{\Delta E}$  will arrive at Ports 4c-7c with equal magnitude and phases of (0°, 0°, 180°, 180°) respectively, and the signal from Port $_{\Delta H}$  will arrive at Ports 4c-7c with equal magnitude and phases of (0°, 180°, 0°, 180°) respectively.

Fig. 8 exhibits the simulated reflection coefficients of all ports of the comparator: below -14 dB and -10 dB for the SUM port and the DIFF ports, respectively, over 30-38 GHz, where the performance of Port $_{\Sigma}$  is more important.

### C. DUAL-POLARIZED RADIATION ELEMENT

The geometry of the radiation element is shown in Fig. 9. The element consists of three layers: the radiation layer, the

V-pol layer and the H-pol layer. The radiation aperture in the radiation layer is a square horn with a size of  $w_{a1} \times w_{a1}$ . By using a structure similar to the orthomode transducer in the V-pol layer and the H-pol layer, horizontal polarization and vertical polarization can be achieved when Port 1r and Port 2r are excited, respectively. In order to broaden the bandwidth, the dimensions of the steps in these two layers are optimized.

The simulated results of the proposed dual-polarized radiation element are shown in Fig. 10. It is seen that the reflection coefficients are lower than -15 dB, and the isolation between the ports of both polarizations is larger than 55 dB within the frequency band of 30-38 GHz.

### D. DUAL-POLARIZED MONOPULSE FEED

The proposed dual-polarized monopulse feed, shown in Fig. 11, consists of the afore-described planar comparators

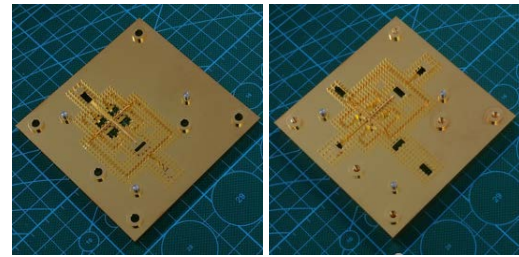
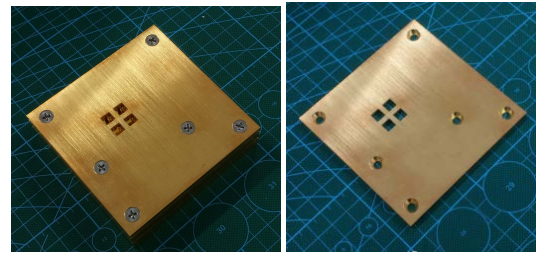
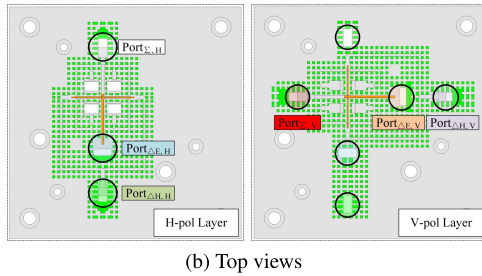
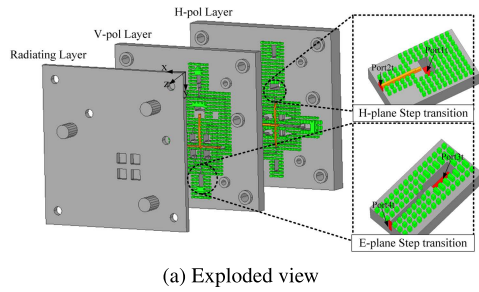


FIGURE 11. Whole geometry of dual-polarized monopulse feed.

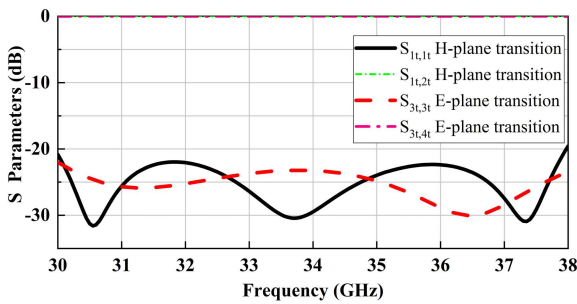
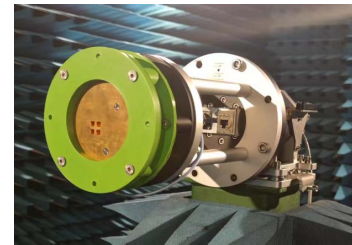


FIGURE 12. Simulated S-parameters of the E-plane and the H-plane step transitions shown in Fig. 11a.

and a  $2 \times 2$  array of the afore-described radiation element with an element spacing of 9 mm in both  $x$ - and  $y$ -axis. The three plates of the monopulse feed can be easily assembled by using several screws without leakage due to the GW characteristics. Step transitions from the RGW and the E-GGW to standard waveguide WR-28 are used for the ports of the feed with simulated reflection coefficients better than  $-20$  dB.

E. PROTOTYPING AND MEASURED RESULTS

The proposed dual-polarized monopulse feed was fabricated by computerized numerical control machining technique. The prototype is shown in Fig. 13, which is made of copper (with electric conductivity  $5.8 \times 10^7 S/m$ ) and gold-plated. The manufacture tolerance is 0.02 mm. The total size is  $75 \times 75 \times 20$  mm<sup>3</sup>. The S-parameters were measured by using an Agilent E8363B vector network, and the radiation characteristics of the antenna were measured in a far-field range test setup, at Gapwaves AB and Chalmers University of Technology, both in Gothenburg. The simulated and measured gains of the SUM-patterns are shown in Fig. 14, where the measured gain  $G_{mea}$  is obtained by comparison



(e) Measurement setup at Chalmers

FIGURE 13. Prototype and measurement setup of dual-polar monopulse feed.

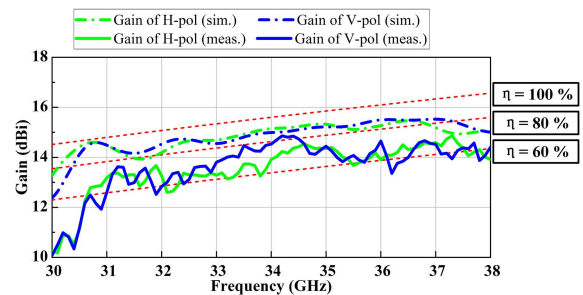
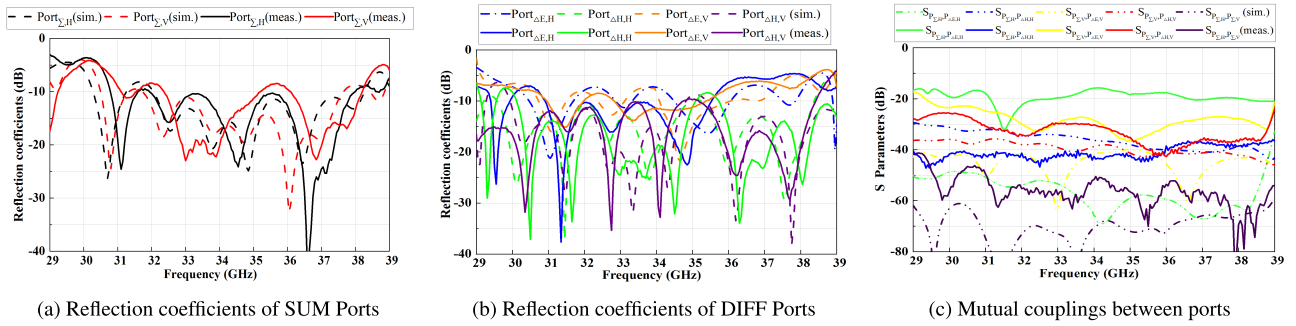
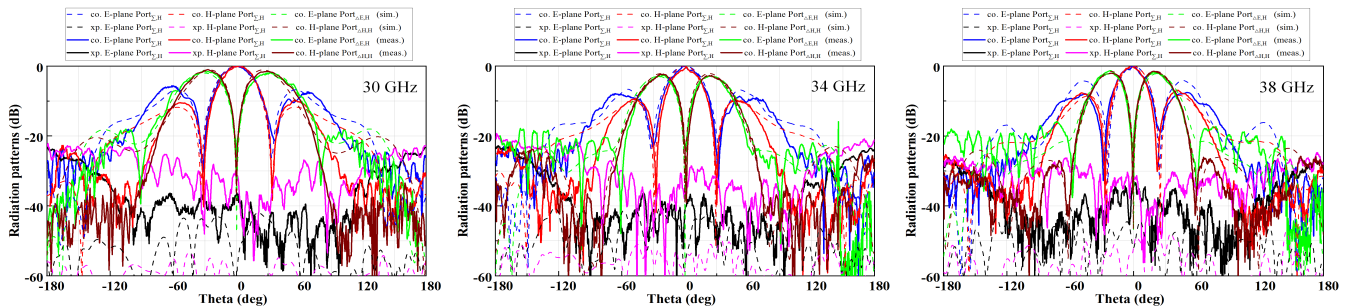


FIGURE 14. Simulated and measured gains of dual-polarized monopulse feed.

method with a standard horn antenna. Then, the measured antenna efficiency  $e_{ant,mea}$  is obtained by  $e_{ant,mea} = G_{mea} / D_{max}$ , where  $D_{max}$  is the theoretical maximum available directivity of the antenna with the aperture size of  $18 \times 18$  mm<sup>2</sup>. The measured gains follow the simulated ones, though there are 2 dB gain differences (about 10% difference in total antenna efficiency) on average. We believe that this difference is due to that the surface roughness of the prototype which was not included in the simulation. The overall measured antenna efficiency is above 60% except at few points. The simulated and measured S-parameters are compared in Fig. 15. It is



**FIGURE 15.** S-parameters of Prototype of dual-polarized monopulse feed, where  $\Sigma$  stands for SUM,  $\Delta$  for DIFF, and  $H$  and  $V$  for horizontal and vertical polarization, respectively.



**FIGURE 16.** Simulated and measured radiation patterns of the proposed feed for Hor-Polar  $\text{Port}_{\Sigma H}$ ,  $\text{Port}_{\Delta EH}$  and  $\text{Port}_{\Delta HH}$ .

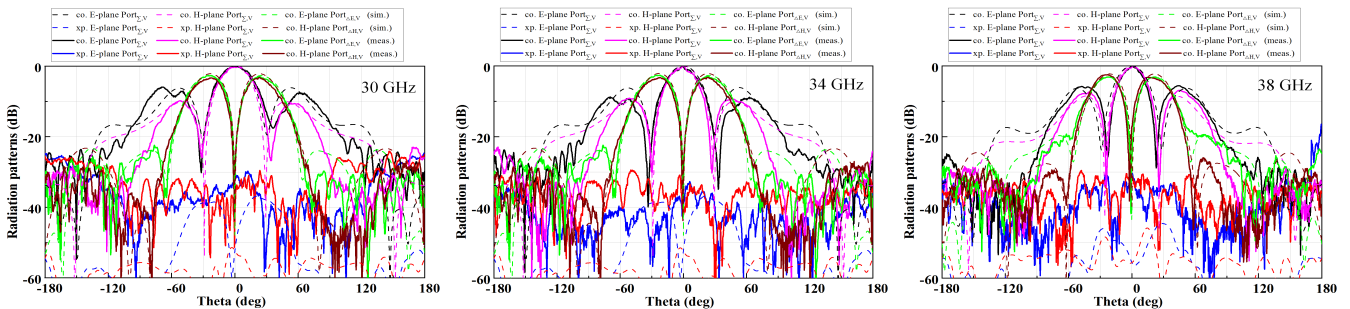


**FIGURE 17.** Simulated and measured radiation patterns of the proposed feed for Ver-Polar  $\text{Port}_{\Sigma V}$ ,  $\text{Port}_{\Delta EV}$  and  $\text{Port}_{\Delta HV}$ .

**TABLE 1.** Key Performance Comparison between Our Proposed Feed and Other Reported Designs.

Ref	Comparator type	Transmission lines	Bandwidth	Center frequency	Gain	Polarization	Type
[3]	magic-T	groove GW	21%	95 GHz	30.5 dBi	single LP	planar array antenna
[5]	magic-T	SIW	13.1%	60 GHz	15.8 dBi	single LP	planar array antenna
[6]	magic-T	waveguide (WG)	21.7%	90 GHz	13.5 dBi	single LP	feed for reflectors
[9]	coupler&phase shifter	waveguide (WG)	4.3%	94 GHz	36.1 dBi	dual CP	planar array antenna
[10]	magic-T	3D print WG	12.9%	15 GHz	31.5 dBi	single LP	planar array antenna
this work	planar magic-T	groove&ridge GW	20.9%	34 GHz	15.5 dBi	dual LP	feed for reflectors

seen that the measured reflection coefficients at SUM-ports are below  $-10$  dB and  $-8$  dB over the frequency band of  $30.8 - 38$  GHz for horizontal and vertical polarizations, respectively. For Diff ports, the reflection coefficient specification is relaxed to  $-5$  dB and the measured data has fulfilled the specification, because the deep difference patterns' null

dips are more important. The simulated mutual couplings between different ports within the entire frequency band are below  $-30$  dB. It is noted that the measured mutual couplings between the SUM-ports and the DIFF-ports are worse than the simulations, especially between  $\text{Port}_{\Sigma H}$  and  $\text{Port}_{\Delta EH}$  with the values about  $-15$  dB, due to an asymmetrical fabrication

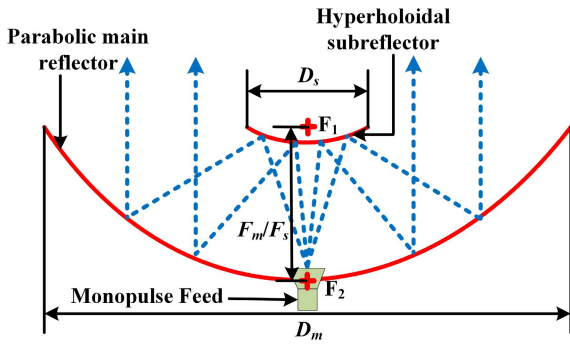


**FIGURE 18.** Dual-reflector Cassegraine antenna with monopulse feed. Reflectors parameters: diameter of main reflector  $D_m = 1.6$  m, diameter of sub-reflector  $D_s = 0.4$  m, focal diameter ratio of main reflector  $F_m = 0.4$ , focal diameter ratio of sub-reflector  $F_s = 0.4$ , eccentricity of sub-reflector  $e = 1.5$ .

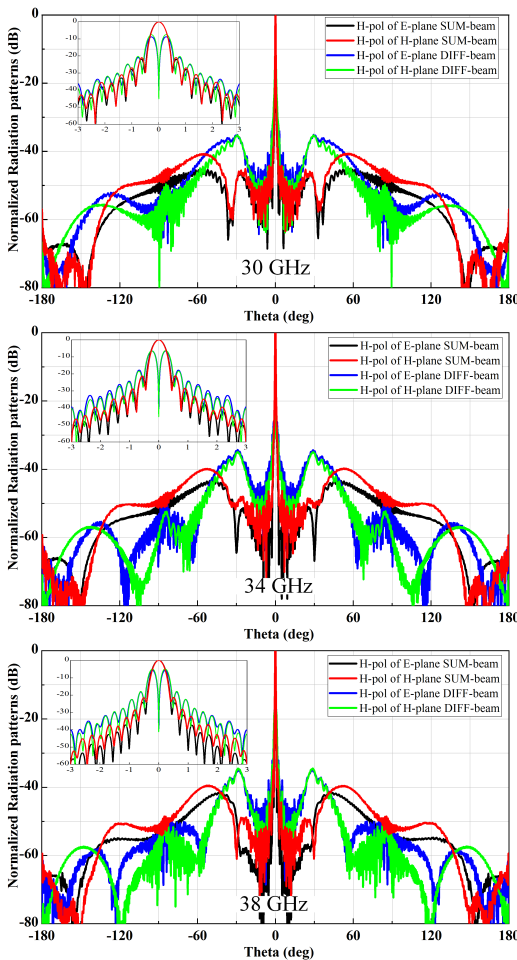


**FIGURE 19.** Simulated normalized radiation patterns for horizontal polarization of Cassegraine dual-reflector antenna.

error of SUM port RGW location in DIFF port E-GGW in 3(RGW)+(E-GGW) Magic T. This asymmetry does not affect the DIFF pattern null depth. Figs. 16 and 17 show the simulated and measured radiation patterns in E- and H-planes of the feed at 30, 34, and 38 GHz for both horizontal and

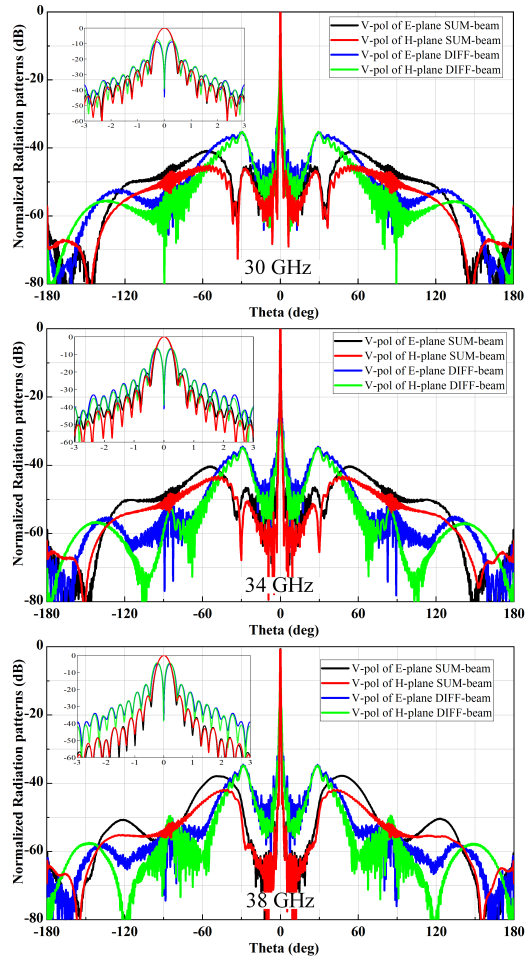


**FIGURE 20.** Simulated normalized radiation patterns for vertical polarization of Cassegraine dual-reflector antenna.

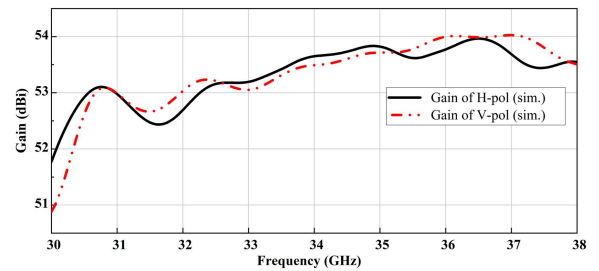


**FIGURE 21.** Simulated gain of SUM-beams of the Cassegraine dual-reflector antenna.

vertical polarizations. The simulated relative null depth in DIFF patterns (the dB value below the maximum of SUM patterns) is around  $-40$  dB. All measured DIFF patterns' relative null depths are below  $-30$  dB. These measured results indicate that the proposed feed achieves a good monopulse performance in dual-polarization and in both E- and H-planes within the whole band.

Key performance of some reported planar monopulse antennas and monopulse feeds have been summarized in Table 1 as a comparison with our proposed feed. Compared

with the single polarized feeds in [5] and [6], our feed introduces a new planar magic-T and simplifies an existing planar magic-T by combining E-GGW with RGW to make a compact monopulse structure for dual polarization with a wide bandwidth. Due to the utilization of the combined GW technology, the proposed feed exhibits a good performance over a wide bandwidth with a simpler structure for assembling and lower manufacturing cost than those feeds in [5] and [6].

### III. PRELIMINARY DESIGN OF ULTRA-HIGH-GAIN REFLECTOR ANTENNA

A dual-reflector Cassegraine antenna, consisting of a paraboloidal main reflector, a hyperboloidal sub-reflector and the dual-polarized monopulse GW feed as shown in Fig. 18, is employed in this work to achieve 50 dBi antenna gain. A preliminary design is done by using GRASP, and antenna parameters are listed in the caption of Fig. 18.

The simulated radiation performance of the whole reflector antenna is obtained by using GRASP with the CST simulated (verified by measurements) far-field function of the feed as the input to GRASP. The radiation patterns in E- and H-planes for horizontal and vertical polarizations are shown in Figs. 19 and 20 at 30, 34 and 38 GHz. The gain of the SUM-beam within the operating frequency range of 30-38 is shown in Fig. 21. It is seen that the simulated gains of SUM-beams are higher than 50 dBi and is 53.4 dBi at 34 GHz, and the first relative sidelobe level is below -22 dB. The DIFF-beam null depth is below -34.7 dB relative to the maximum of SUM-beams. The gain difference between SUM- and DIFF-patterns is about 6 dB. All the mentioned data are the results after considering the blockage of the sub-reflector, modelled in GRASP. The simulated results verify the design of the dual-polarized monopulse feed preliminarily and numerically.

### IV. CONCLUSION

In this paper, a dual-polarized monopulse feed, composed of three contactless plates, has been proposed based on gap waveguide technology with two types of planar GW magic tees to form a monopulse comparator. Due to the separate plates, the manufacture cost has been reduced a lot with a low-loss characteristic, where the assembly tolerance is relatively easy to be guaranteed. The feed has been designed and manufactured. The measurements of the prototype have verified the design of the feed. Finally, the designed feed is used to feed a dual-reflector Cassegraine antenna with the simulations of numerical modeling in GRASP to achieve an ultra-high gain of above 50 dBi with 2D tracking functions. The proposed antenna is aiming to be used in 5G mmWave backhauling systems.

### ACKNOWLEDGMENT

The authors would like to thank Hanna Karlsson for her help in measurements at Gapwaves AB.

### REFERENCES

- [1] J. Du, E. Onaran, D. Chizhik, S. Venkatesan, and R. A. Valenzuela, "Gbps user rates using mmWave relayed backhaul with high-gain antennas," *IEEE J. Sel. Areas Commun.*, vol. 35, no. 6, pp. 1363–1372, Jun. 2017.
- [2] U. Nickel, "Overview of generalized monopulse estimation," *IEEE Aerosp. Electron. Syst. Mag.*, vol. 21, no. 6, pp. 27–56, Jun. 2006.
- [3] A. Vosoogh, A. Haddadi, A. U. Zaman, J. Yang, H. Zirath, and A. A. Kishk, "W-band low-profile monopulse slot array antenna based on gap waveguide corporate-feed network," *IEEE Trans. Antennas Propag.*, vol. 66, no. 12, pp. 6997–7009, Dec. 2018.
- [4] Y. J. Cheng, W. Hong, and K. Wu, "94 GHz substrate integrated monopulse antenna array," *IEEE Trans. Antennas Propag.*, vol. 60, no. 1, pp. 121–129, Jan. 2012.
- [5] J. Zhu, S. Liao, S. Li, and Q. Xue, "60 GHz substrate-integrated waveguide-based monopulse slot antenna arrays," *IEEE Trans. Antennas Propag.*, vol. 66, no. 9, pp. 4860–4865, Sep. 2018.
- [6] F. Zhao, Y. J. Cheng, P. F. Kou, and S. S. Yao, "A wideband low-profile monopulse feeder based on silicon micromachining technology for W-band high-resolution system," *IEEE Antennas Wireless Propag. Lett.*, vol. 18, no. 8, pp. 1676–1680, Aug. 2019.
- [7] Y.-X. Zhang, Y.-C. Jiao, L. Zhang, and J.-X. Wen, "Wideband 2-D monopulse antenna array with higher-order mode substrate integrated waveguide feeding and 3-D printed packaging," *IEEE Trans. Antennas Propag.*, vol. 68, no. 4, pp. 3259–3264, Apr. 2020.
- [8] Z. Hao, H. Wang, and W. Hong, "A novel planar reconfigurable monopulse antenna for indoor smart wireless access points' application," *IEEE Trans. Antennas Propag.*, vol. 64, no. 4, pp. 1250–1261, Apr. 2016.
- [9] P. Zheng, G. Q. Zhao, S. H. Xu, F. Yang, and H. J. Sun, "Design of a W-band full-polarization monopulse Cassegrain antenna," *IEEE Antennas Wireless Propag. Lett.*, vol. 16, pp. 99–103, 2016.
- [10] G.-L. Huang, S.-G. Zhou, and T.-H. Chio, "Highly-efficient self-compact monopulse antenna system with integrated comparator network for RF industrial applications," *IEEE Trans. Ind. Electron.*, vol. 64, no. 1, pp. 674–681, Jan. 2017.
- [11] P. Zheng, B. Hu, S. Xu, and H. Sun, "A W-band high-aperture-efficiency multipolarized monopulse Cassegrain antenna fed by phased microstrip patch quad," *IEEE Antennas Wireless Propag. Lett.*, vol. 16, pp. 1609–1613, 2017.
- [12] B. Liu, W. Hong, Z. Kuai, X. Yin, G. Luo, J. Chen, H. Tang, and K. Wu, "Substrate integrated waveguide (SIW) monopulse slot antenna array," *IEEE Trans. Antennas Propag.*, vol. 57, no. 1, pp. 275–279, Jan. 2009.
- [13] H. Chu, J.-X. Chen, S. Luo, and Y.-X. Guo, "A millimeter-wave filtering monopulse antenna array based on substrate integrated waveguide technology," *IEEE Trans. Antennas Propag.*, vol. 64, no. 1, pp. 316–321, Jan. 2016.
- [14] C. Guo, J. Li, Y. Yu, F. Zhang, Y. Zhu, Q. Yang, W. Zhu, and S. Zhu, "A 3-D printed E-plane waveguide magic-T using air-filled coax-to-waveguide transitions," *IEEE Trans. Microw. Theory Techn.*, vol. 67, no. 12, pp. 4984–4994, Dec. 2019.
- [15] W. Feng, W. Che, and K. Deng, "Compact planar magic-T using E-plane substrate integrated waveguide (SIW) power divider and slotline transition," *IEEE Microw. Wireless Compon. Lett.*, vol. 20, no. 6, pp. 331–333, Jun. 2010.
- [16] W. Peng, Q. Xiao, and X. Chen, "K-band planar magic-T using LTCC technology," *IEEE Microw. Wireless Compon. Lett.*, vol. 27, no. 8, pp. 715–717, Aug. 2017.
- [17] J. P. Kim and W. S. Park, "Novel configurations of planar multilayer magic-T using microstrip-slotline transitions," *IEEE Trans. Microw. Theory Techn.*, vol. 50, no. 7, pp. 1683–1688, Jul. 2002.
- [18] J. Liu, A. Vosoogh, A. U. Zaman, and J. Yang, "A slot array antenna with single-layered corporate-feed based on ridge gap waveguide in the 60 GHz band," *IEEE Trans. Antennas Propag.*, vol. 67, no. 3, pp. 1650–1658, Mar. 2019.
- [19] T.-L. Zhang, L. Chen, S. M. Moghaddam, A. U. Zaman, and J. Yang, "Millimeter-wave ultrawideband circularly polarized planar array antenna using bold-C spiral elements with concept of tightly coupled array," *IEEE Trans. Antennas Propag.*, vol. 69, no. 4, pp. 2013–2022, Apr. 2021.
- [20] A. Vosoogh, M. S. Sorkherizi, V. Vassilev, A. U. Zaman, Z. S. He, J. Yang, A. A. Kishk, and H. Zirath, "Compact integrated full-duplex gap waveguide-based radio front end for multi-Gbit/s point-to-point backhaul links at E-band," *IEEE Trans. Microw. Theory Techn.*, vol. 67, no. 9, pp. 3783–3797, Sep. 2019.



- [21] J. Liu, A. Vosoogh, A. U. Zaman, and J. Yang, "Design and fabrication of a high-gain 60-GHz cavity-backed slot antenna array fed by inverted microstrip gap waveguide," *IEEE Trans. Antennas Propag.*, vol. 65, no. 4, pp. 2117–2122, Apr. 2017.
- [22] J. L. Vazquez-Roy, A. Tamayo-Dominguez, E. Rajo-Iglesias, and M. Sierra-Castaner, "Radial line slot antenna design with groove gap waveguide feed for monopulse radar systems," *IEEE Trans. Antennas Propag.*, vol. 67, no. 10, pp. 6317–6324, Oct. 2019.
- [23] A. Tamayo-Dominguez, J. Fernández-González, and M. Sierra-Castañer, "3-D-printed modified Butler matrix based on gap waveguide at W-band for monopulse radar," *IEEE Trans. Microw. Theory Techn.*, vol. 68, no. 3, pp. 926–938, Mar. 2020.
- [24] A. Tamayo-Dominguez, J.-M. Fernandez-Gonzalez, and M. Sierra-Castaner, "Monopulse radial line slot array antenna fed by a 3-D-printed cavity-ended modified Butler matrix based on gap waveguide at 94 GHz," *IEEE Trans. Antennas Propag.*, vol. 69, no. 8, pp. 4558–4568, Aug. 2021.
- [25] M. Ferrando-Rocher, J. I. Herranz-Herruzo, A. Valero-Nogueira, B. Bernardo-Clemente, A. U. Zaman, and J. Yang, " $8 \times 8$  Ka-band dual-polarized array antenna based on gap waveguide technology," *IEEE Trans. Antennas Propag.*, vol. 67, no. 7, pp. 4579–4588, Jul. 2019.
- [26] M. Guo and F. Yang, "W-band dual polarized array antenna based on gap waveguide technology," in *Proc. IEEE Asia-Pacific Microw. Conf. (APMC)*, Dec. 2020, pp. 317–319.
- [27] TICRA. [Online]. Available: <https://www.ticra.com/software/grasp/>
- [28] CST Microwave Studio. [Online]. Available: <http://www.cst.com>
- [29] Y.-J. He, D.-Y. Mo, Q.-S. Wu, and Q.-X. Chu, "A Ka-band waveguide magic-T with coplanar arms using ridge-waveguide transition," *IEEE Microw. Wireless Compon. Lett.*, vol. 27, no. 11, pp. 965–967, Nov. 2017.
- [30] A. Farahbakhsh, "Ka-band coplanar magic-T based on gap waveguide technology," *IEEE Microw. Wireless Compon. Lett.*, vol. 30, no. 9, pp. 853–856, Sep. 2020.



**ENLIN WANG** received the B.S. degree in electronic engineering from the Henan University of Technology, Zhengzhou, China, in 2018. She is currently pursuing the Ph.D. degree with Xidian University. She is currently a Guest Ph.D. Student at the Chalmers University of Technology. Her current research interests include the gap waveguide technology, mmWave antennas, and reflector antennas.



**TIANLING ZHANG** (Member, IEEE) received the B.Sc. degree in electromagnetic engineering, and the M.Sc. and Ph.D. degrees in electromagnetic fields and microwave technology from Xidian University, Xi'an, China, in 2004, 2007, and 2011, respectively.

From 2018 to 2019, he was a Visiting Researcher with the Chalmers University of Technology, Gothenburg, Sweden. He is currently an Associate Professor with the National Key Laboratory of Antennas and Microwave Technology, Xidian University. His research interests include wideband millimeter-wave planar array antennas, phased array antennas, reflector antennas, and microwave passive components.



**ASHRAF UZ ZAMAN** (Senior Member, IEEE) was born in Chittagong, Bangladesh. He received the M.Sc. and Ph.D. degrees from the Chalmers University of Technology, Gothenburg, Sweden, in 2007 and 2013, respectively. He is currently an Associate Professor with the Communication and Antenna Systems Division, Chalmers University of Technology. His current research interests include high gain millimeter-wave planar antennas, gap waveguide technology, frequency-selective surfaces, microwave passive components, RF packaging techniques, and low-loss integration of MMICs with the antennas.



**THOMAS EMANUELSSON** (Member, IEEE) received the M.Sc. degree in electronic engineering from the Chalmers University of Technology, in 1984. He is currently holding a position as an Expert in microwave technology at Ericsson AB and an Adjunct Professor at the Microwave Electronics Laboratory, Department of Microtechnology and Nanoscience (MC2), Chalmers University of Technology. His research interests include mmWave radio communication, radar phased array systems, and MMIC technology.



**PER-ARNE THORSEN** received the M.S. degree in electrical engineering from the Chalmers University of Technology, Gothenburg, Sweden, in 1983. He is currently holding a position as a Technology Specialist within the area of wireless transport at Ericsson AB, Gothenburg.



**SAM AGNEESSENS** received the M.S. and Ph.D. degrees in electrical engineering from Ghent University, Belgium, in 2011 and 2015, respectively.

He was a Postdoctoral Fellow of the Research Foundation-Flanders (FWO-V) affiliated with Ghent University and imec, and became an Assistant Professor at Ghent university, in 2017. In 2018, he joined Ericsson AB, Gothenburg, Sweden, as a Senior Researcher. He currently leads the wireless transport research project at Ericsson. His research interests include electromagnetics focusing on robust antenna systems for wearable applications and mmWave systems.

Dr. Agneessens received the URSI Young Scientist Award from the 2014 URSI General Assembly and was awarded the 2014 Premium Award for Best Paper in *IET Electronics Letters*.



**JIAN YANG** (Senior Member, IEEE) received the B.S. degree in electrical engineering from the Nanjing University of Science and Technology, Nanjing, China, in 1982, the M.S. degree in electrical engineering from the Nanjing Research Center of Electronic Engineering, Nanjing, in 1985, and the Swedish Licentiate and Ph.D. degrees from the Chalmers University of Technology, Gothenburg, Sweden, in 1998 and 2001, respectively. From 1985 to 1996, he was with the Nanjing Research Institute of Electronics Technology, Nanjing, as a Senior Engineer. From 1999 to 2005, he was with the Department of Electromagnetics, Chalmers University of Technology, as a Research Engineer. During 2005 and 2006, he was with Comhat AB, as a Senior Engineer. From 2006 to 2010, he was an Assistant Professor at the Department of Signals and Systems, Chalmers University of Technology. In 2010, 2016, and 2020, he was an Associate Professor, a Professor, and a Full Professor, respectively, at the Department of Electrical Engineering, Chalmers University of Technology. He has published more than 80 journal articles and about 200 peer reviewed conference papers. H-index: 31 and i10-index: 80.

His research interests include ultra-wideband antennas and UWB feeds for reflector antennas, mmWave antennas, mmWave multilayer phased array antennas, mmWave SWE (sheet waveguide element) antennas, gap waveguide antennas, UWB radar systems, UWB antennas in near-field sensing applications, hat-fed antennas, reflector antennas, radome design, and computational electromagnetics.

...